Developmental Cell
Article

LRF Is an Essential Downstream Target of GATA1 in Erythroid Development and Regulates BIM-Dependent Apoptosis

Takahiro Maeda,[1,2,7,8] Keisuke Ito,[1,2,3,8] Taha Merghoub,[1,2] Laura Poliseno,[1,2,3] Robin M. Hobbs,[1,2,3] Guocan Wang,[1,2,3] Lin Dong,[1,2] Manami Maeda,[1,2,7] Louis C. Dore,[4] Arthur Zelent,[5] Lucio Luzzatto,[1,2,6] Julie Teruya-Feldstein,[2] Mitchell J. Weiss,[4] and Pier Paolo Pandolfi[1,2,3,*]

[1]Cancer Biology and Genetics Program
[2]Department of Pathology
Sloan-Kettering Institute, Memorial Sloan-Kettering Cancer Center, 1275 York Avenue, New York, NY 10021, USA
[3]Cancer Genetics Program, Beth Israel Deaconess Cancer Center, Departments of Medicine and Pathology, Beth Israel Deaconess Medical Center, Harvard Medical School, 330 Brookline Avenue, Boston, MA 02215, USA
[4]Children's Hospital of Philadelphia, Division of Hematology, University of Pennsylvania, Philadelphia, PA 19104, USA
[5]Leukemia Research Fund Center at the Institute of Cancer Research, Chester Beatty Laboratories, London SW3 6JB, UK
[6]Istituto Toscano Tumori, 50139 Firenze, Italy
[7]Present address: Department of Hematopoietic Stem Cell and Leukemia Research, Beckman Institute of the City of Hope, 1500 East Duarte Road, Duarte, CA 91010, USA
[8]These authors contributed equally to this work
*Correspondence: ppandolf@bidmc.harvard.edu
DOI 10.1016/j.devcel.2009.09.005

SUMMARY

GATA-1-dependent transcription is essential for erythroid differentiation and maturation. Suppression of programmed cell death is also thought to be critical for this process; however, the link between these two features of erythropoiesis has remained elusive. Here, we show that the POZ-Krüppel family transcription factor, LRF (also known as Zbtb7a/Pokemon), is a direct target of GATA1 and plays an essential antiapoptotic role during terminal erythroid differentiation. We find that loss of *Lrf* leads to lethal anemia in embryos, due to increased apoptosis of late-stage erythroblasts. This programmed cell death is Arf and p53 independent and is instead mediated by upregulation of the proapoptotic factor *Bim*. We identify *Lrf* as a direct repressor of *Bim* transcription. In strong support of this mechanism, genetic *Bim* loss delays the lethality of *Lrf*-deficient embryos and rescues their anemia phenotype. Thus, our data define a key transcriptional cascade for effective erythropoiesis, whereby GATA-1 suppresses BIM-mediated apoptosis via LRF.

INTRODUCTION

Production of red blood cells (RBCs) is normally maintained at a constant level by a finely tuned regulation of erythropoiesis. During terminal maturation, mammalian erythroblasts extrude their nuclei and give rise to RBCs. Over the past 20 years a wealth of experimental evidence has unveiled the role of critical genes during erythropoiesis (Godin and Cumano, 2002). In particular, lineage-specific transcription factors and cytokines regulate erythroid cell fate by activating or inactivating key factors for cellular differentiation and survival. The nuclear protein GATA1 is highly expressed in the erythroid lineages and activates the transcription factor Eklf (Crossley et al., 1994; Welch et al., 2004) along with many other erythroid-specific genes. Disruption of the *Gata1* gene in mice causes embryonic lethality due to defects in yolk sac primitive erythropoiesis (Fujiwara et al., 1996). Furthermore, hematopoietic differentiation of *Gata1*-null embryonic stem (ES) cells in vitro revealed a block of differentiation at the proerythroblast stage due to developmental arrest and apoptosis (Weiss et al., 1994), indicating that Gata1 also plays a key role in definitive erythropoiesis. How GATA1 regulates differentiation and survival of immature erythroblasts is not fully understood. The GATA1 target EKLF acts primarily as a transcriptional activator and induces multiple erythroid-specific genes (Hodge et al., 2006). *Eklf*-knockout mice die of severe anemia by 16.5 days postcoitum (d.p.c.) due to defective definitive erythropoiesis (Perkins et al., 1995). Erythropoietin (EPO) and its receptor (EPO-R) are also essential for RBC production and deliver key signals for erythroid cell survival (Richmond et al., 2005). EPO activates multiple signaling pathways and induces the antiapoptosis factor Bcl-X_L (Richmond et al., 2005; Socolovsky et al., 1999). Both *Epo*- and *Epo-R*-knockout mice are embryonic lethal due to a lack of definitive erythropoiesis (Wu et al., 1995).

LRF (encoded by the *ZBTB7a* gene, formerly described as POKEMON [Davies et al., 1999; Maeda et al., 2005], FBI-1 [Pessler et al., 1997], and OCZF [Kukita et al., 1999]) is a transcription factor that belongs to the POK (POZ/BTB and Krüppel) protein family. POK proteins bind DNA through C-terminal Krüppel-type zinc fingers and recruit corepressor complexes through the N-terminal POZ/BTB domain (Stogios et al., 2005). POK proteins act as transcriptional repressors and play important roles in cellular differentiation and oncogenesis (Costoya et al., 2004; He et al., 2005). We previously reported that Lrf can act

as a proto-oncogene through repression of *Arf*: specifically, Lrf can trigger lymphomagenesis in the mouse and it is markedly overexpressed in non-Hodgkin's lymphoma cells (Maeda et al., 2005). We have also shown that LRF critically regulates B versus T lymphocyte fate decisions by opposing the Notch signaling pathway. Conditional loss of *Lrf* in adult hematopoietic stem cells (HSCs) results in the aberrant development of bone marrow (BM) CD4/CD8 double-positive T cells, at the expense of B cell development (Maeda et al., 2007). Here we show that Lrf exerts an essential role for the biology of erythroid precursors. We demonstrate that Lrf acts downstream of Gata1 by suppressing Bim-mediated apoptosis, thus ensuring continued production of RBCs.

RESULTS

Lrf Is Required for Definitive Fetal Erythropoiesis

Zbtb7a$^{+/-}$ mutants (Maeda et al., 2005) were seemingly healthy and fertile, but intercrossing did not produce any live *Zbtb7a*$^{-/-}$ progeny. When we analyzed embryos from timed pregnancies of *Zbtb7a*$^{+/-}$ intercrosses, we found that until 12.5 d.p.c. the null embryos were present at normal Mendelian ratio and most of them had no gross morphological abnormalities (not shown). However, by 14.5 d.p.c. the peripheral blood (PB) from *Zbtb7a*$^{-/-}$ embryos revealed large numbers of erythroblasts at the polychromatophilic to orthochromic stage, as though their further maturation was blocked: indeed, there were very few mature red cells (Figure 1C, top). All *Zbtb7a*$^{-/-}$ embryos died between 15.5 and 16.5 d.p.c. This was likely due to anemia as indicated by severe pallor and a marked reduction in the hematocrit (Figure 1A and 1B). Moreover, touch preparations of 14.5 d.p.c. fetal liver (FL) demonstrated a lack of enucleated erythrocytes and a preponderance of immature precursors (Figure 1C, bottom). Because the 14.5 d.p.c. FL cell compartment consists mainly of erythroblasts, we obtained from each genotype total FL cell counts; these were significantly reduced in *Zbtb7a*$^{-/-}$ embryos (Figure 1D). Furthermore, differential counts demonstrated in *Zbtb7a*$^{-/-}$ embryos a severe decrease in polychromatophilic and orthochromatophilic erythroblasts, as well as in erythrocytes (Figure 1E). Stages of erythroid development can be characterized by flow cytometric analysis (FACS) on the basis of expression of Ter119 and CD71. As shown in Figure S1 (available online), the CD71^{+}Ter119^{-} population (R1) consists mainly of proerythroblasts and early basophilic erythroblasts, whereas the CD71^{+}Ter119^{+} population (R2) is composed of basophilic erythroblasts and early polychromatophilic erythroblasts. The CD71^{-}Ter119^{+} population (R3) is a more heterogeneous population and consists of poly/orthochromatophilic erythroblasts and enucleated erythrocytes. FACS analysis revealed a severe defect in terminal erythroid differentiation in *Zbtb7a*$^{-/-}$ FLs (Figure 1F). Proportions of R2 and R3 were significantly decreased in *Zbtb7a*$^{-/-}$ FLs, whereas R1 was barely affected (Figure 1F). This observation was more evident in later embryonic days (14.5 d.p.c.), in which exponential expansion of mature erythroblasts occurs (Figure 1F). In addition, purified *Zbtb7a*$^{-/-}$ erythroblasts from each stage, particularly the later ones, exhibited a less condensed chromatin pattern compared with wild-type embryos (Figure S1). Therefore, loss of *Lrf* causes lethal embryonic anemia with impaired erythroid maturation. This severe anemia is not due to lack of erythroid progenitors, as shown by colony assays from 13.5 d.p.c. FL (Figure 1G). However, whereas *Zbtb7a*$^{+/+}$ colonies were largely composed of mature erythrocytes, CFU-E colonies from *Zbtb7a*$^{-/-}$ mutants did not contain mature enucleated cells (Figure 1G right). In order to verify the cell intrinsic nature of this phenotype, we introduced an Lrf retroviral vector in *Zbtb7a*$^{-/-}$ early erythroblasts, followed by differentiation in vitro. As shown in Figure 1H, Lrf almost completely rescued the differentiation defect in *Zbtb7a*$^{-/-}$ cells. Lrf-infected erythroblasts (GFP positive), but not GFP negative cells, successfully differentiated into Ter119-positive, small, mature erythroblasts in vitro.

Conditional Ablation of *Lrf* in the Adult Causes an EPO-Unresponsive Macrocytic Anemia

To further elucidate the role of LRF in erythropoiesis, we next produced *Lrf* conditional knockout mice (Maeda et al., 2007) and made use of Mx1-Cre transgenic mice, in which Cre recombinase can be induced specifically in HSCs by the administration of polyinosinic-polycytidylic acid (pIpC) (Kuhn et al., 1995). In *Zbtb7a*$^{Flox/FloxMx1cre+}$ mice, RBC and hematocrit gradually decreased after pIpC administration, whereas their mean corpuscular volume (MCV) increased, suggesting that erythropoiesis was abnormal not only quantitatively but also qualitatively (Figure 2A). One month after pIpC injection we found that serum EPO levels in pIpC-treated *Zbtb7a*$^{Flox/FloxMx1cre+}$ mice were in fact high (Figure 2B), reflecting an appropriate physiological response to the anemia caused by loss of *Lrf*. FACS analysis in BM and spleen demonstrated that mature erythroblasts and erythrocytes (R IV) (Socolovsky et al., 2001) were dramatically decreased, while the early erythroblast compartment (R II) was expanded in *Lrf* conditional knockout mice (Figure 2C); thus these mice displayed an erythroid defect specifically at the transition from R II to III/IV, which corresponds to basophilic erythroblasts and poly/orthochromatic erythroblasts, respectively, consistent with our findings in *Lrf* knockout embryos. Splenomegaly in pIpC-treated *Zbtb7a*$^{Flox/FloxMx1cre+}$ mice is most likely due to a compensatory expansion of the early erythroid compartment that is negative for Lrf (Figure 2D and Figure S2A). In the BM of these mice, absolute numbers of MEPs (megakaryo-erythrocytic progenitors) were increased (Figure 2E) and they gave rise to comparable numbers of CFU-E colonies as the controls (Figure 2F), suggesting that loss of *Lrf* does not affect erythroid lineage commitment.

Anemia triggered by conditional inactivation of *Lrf* was even more evident in a transplant model (Figure S2B). However, recipients with BM reconstituted from *Zbtb7a*$^{Flox/-Mx1cre+}$ cells developed severe macrocytic anemia upon pIpC administration (Figure S2C). Taken together, these data support the notion that the anemia in *Lrf* conditional knockout mice is caused by a cell-intrinsic mechanism.

We next examined how *Lrf* conditional knockout mice would respond to a severe hemolytic stress. Upon treatment with the potent hemolytic agent phenylhydrazine (PHZ: see Socolovsky et al., 2001), *Lrf*-ablated mice developed more severe anemia than control mice; also, they had a delayed reticulocyte response (Figure 2G) and a striking increase of PB mononuclear cells (MNCs), which consisted almost exclusively of nucleated Lrf-deficient erythroblasts (Figures 2H, S2D, and S2E). We conclude that upon hemolytic stress, *Lrf* conditional knockout mice were

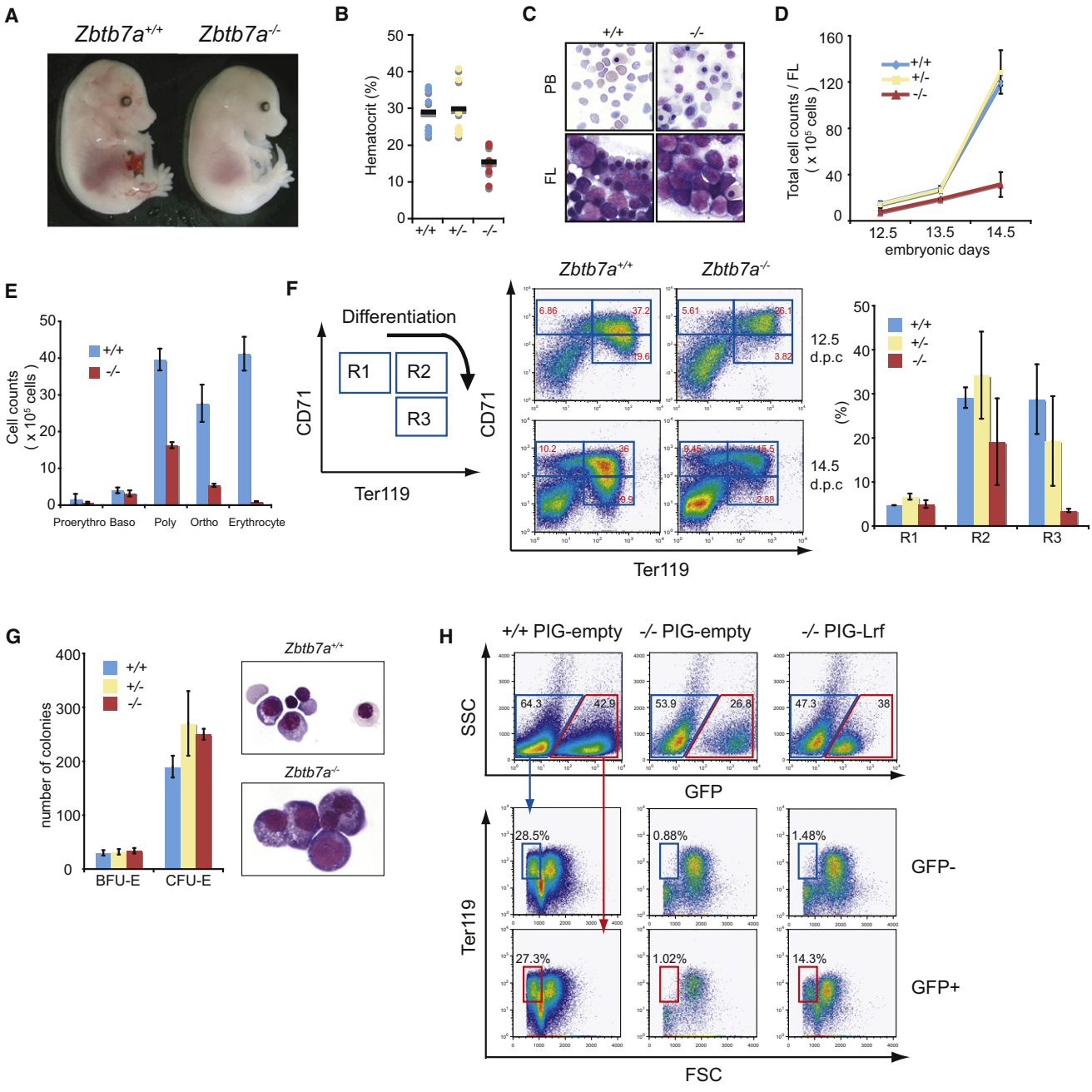

Figure 1. Loss of *Lrf* Results in Embryonic Lethality due to Severe Anemia

(A) Picture of *Zbtb7a*$^{+/+}$ and *Zbtb7a*$^{-/-}$ 15.5 d.p.c. embryos.

(B) Hematocrit of *Zbtb7a*$^{+/+}$, *Zbtb7a*$^{+/-}$, and *Zbtb7a*$^{-/-}$ littermate embryos at 15.5 d.p.c.

(C) PB and FL touch preparation from *Zbtb7a*$^{+/+}$ and *Zbtb7a*$^{-/-}$ littermate embryos at 14.5 d.p.c.

(D) Total cell numbers per FL for each genotype at different embryonic days.

(E) Differential counts on FL cells from *Zbtb7a*$^{+/+}$ and *Zbtb7*$^{-/-}$ littermate embryos.

(F) Representative FACS profiles of 12.5 d.p.c. and 14.5 d.p.c. FLs from *Zbtb7a*$^{+/+}$ and *Zbtb7a*$^{-/-}$ embryos. Bar graph represents proportions of each population in 12.5 d.p.c. FLs.

(G) Colony counts of in vitro differentiated FL precursors derived from 13.5 d.p.c. littermate embryos (left). Pictures demonstrate cytospin preparations of CFU-E colonies from *Zbtb7a*$^{+/+}$ (top) and *Zbtb7a*$^{-/-}$ FLs (bottom).

(H) Lrf add-back into *Zbtb7a*$^{-/-}$ erythroblasts rescued impaired differentiation phenotype in vitro. Both *Zbtb7a*$^{+/+}$ and *Zbtb7a*$^{-/-}$ immature erythroblasts (Ter119^{-}Gr1^{-}B220^{-}) were isolated from 12.5 d.p.c. FLs and infected with either MSCV-Puro-IRES-GFP (PIG) empty vector or PIG-Lrf vector (Maeda et al., 2005). We then induced erythroid differentiation in vitro and subsequently analyzed for Ter119 expression and cell size (forward scatter: FSC) by FACS. All error bars indicate standard deviation (SD).

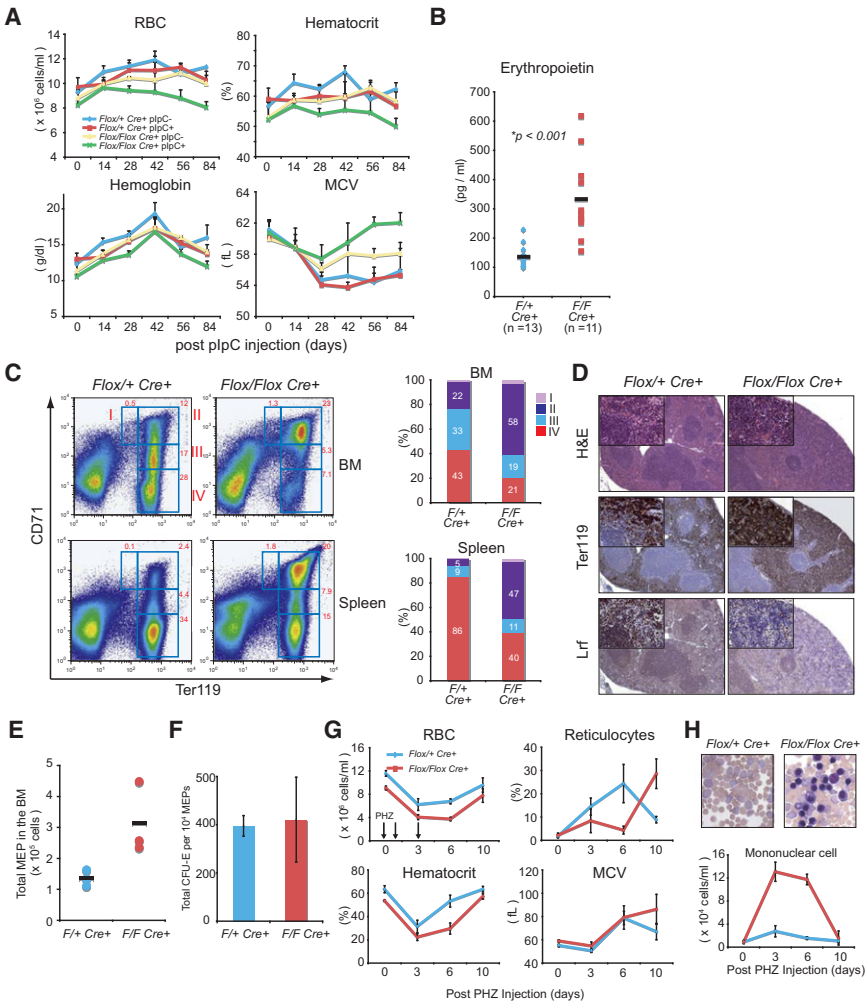

Figure 2. Ablation of *Lrf* in the Hematopoietic Compartment of Adult Mice Results in Macrocytic Anemia and Ineffective Erythropoiesis

(A) We examined four different groups of mice according to genotype and treatment: $Zbtb7a^{Flox/+Mx1cre+}$ PBS treated (blue), $Zbtb7a^{Flox/+Mx1cre+}$ plpC treated (red), $Zbtb7a^{Flox/FloxMx1cre+}$ PBS treated (yellow), and $Zbtb7a^{Flox/FloxMx1cre+}$ plpC-treated (green). RBC counts, hematocrit, hemoglobin, and MCV in PB were measured by a hematology analyzer. The average of five animals was plotted at each time point with error bars.

(B) Serum EPO level 1 month after plpC injection.

(C) Representative FACS profiles for Ter119 and CD71 expression in BM and spleen 1 month after plpC administration (left). Bar graphs represent percent of each population in BM and spleen (right).

(D) Representative hematoxylin and eosin staining of spleen sections (top), demonstrating expansion of red pulp formation in the spleen of plpC-treated $Zbtb7a^{Flox/FloxMx1cre+}$ mice (middle panels for Ter119 and bottom panels for Lrf staining).

(E) Absolute numbers of megakaryocyte/erythroid progenitors (MEPs) in the BM 1 month after plpC administration. Black bars resent the average cell counts of three mice.

(F) Erythroid colony-forming capacity per 10,000 flow-sorted MEPs was assessed in three independent mice for each genotype.

(G) RBC counts, hematocrit, and MCV were measured in the PB on indicated days after PHZ treatment. Reticulocytes were counted on PB smear slides upon new methylene blue staining.

(H) Robust increase of PB MNCs in PHZ-treated, plpC-pretreated $Zbtb7a^{Flox/FloxMx1cre+}$ mice (bottom). Pictures demonstrate Wright-Giemsa staining of PB on day 3. All error bars indicate SD.

able to mobilize immature nucleated erythroblasts from BM and spleen into the peripheral blood, but they suffered even more anemia than control mice.

Loss of *Lrf* Triggers *Arf/p53*-Independent Apoptosis during Late Stages of Erythroid Development

To further elucidate the mechanism by which loss of *Lrf* causes ineffective erythropoiesis, we first analyzed the cell cycle in $Zbtb7a^{-/-}$ FLs. As shown in Figure S2F, we found in FLs of these mice a relative increase of cells in G1 and a concomitant decrease of cells in S and G_2/M. Next we looked for evidence of apoptosis and found a dramatic increase of Annexin V-positive apoptotic cells (Figure 3A); this was so pronounced, particularly in the later stage of erythroid differentiation (R2), that we suggest it could account for the lethal anemia of $Zbtb7a^{-/-}$ embryos.

Because loss of the tumor suppressor *Arf* reverted the senescence phenotype in $Zbtb7a^{-/-}$ MEFs (mouse embryonic fibroblasts) (Maeda et al., 2005) and $p19^{Arf}$ mRNA was only detectable in $Zbtb7a^{-/-}$ $CD71^{+}Ter119^{-}$ erythroblasts by real-time polymerase chain reaction (RT-PCR) (not shown), we next set out to examine whether loss of *Arf* could bypass apoptosis and rescue the anemia phenotype in $Zbtb7a^{-/-}$ embryos. We intercrossed $Zbtb7a^{+/-}p19^{Arf+/-}$ double-heterozygous mice and analyzed FL erythropoiesis in 15.5 d.p.c. embryos. As shown in Figure S3A, $Zbtb7a^{-/-}p19^{Arf-/-}$ embryos still demonstrated a block of differentiation at the R2 stage and total numbers of $Zbtb7a^{-/-}p19^{Arf-/-}$ FL cells were comparable to $Zbtb7a^{-/-}p19^{Arf+/+}$ embryos (Figure S3B).

The tumor suppressor p53 inhibits cellular proliferation by inducing cell cycle arrest and apoptosis in response to cellular stresses such as DNA damage and hypoxia (Fridman and Lowe, 2003). Furthermore, we found that p53 itself is upregulated in $Zbtb7a^{-/-}$ fetal liver erythroblasts (see below). We therefore tested whether genetic inactivation of *p53* could rescue the anemia phenotype of $Zbtb7a^{-/-}$ mice. As shown in Figure S3C, $Zbtb7a^{-/-}p53^{-/-}$ FLs still displayed a block of differentiation. These data suggest that the massive apoptosis at late stages of erythroid differentiation caused by loss of *Lrf* occurs in a $p19^{Arf}$/p53-independent fashion.

Intact EPO Signaling Cascade in *Lrf*-Deficient Erythroblasts

EPO plays a key role in terminal erythroid differentiation by preventing apoptosis in mature erythroblasts. To investigate

whether the loss of *Lrf* impairs EPO signaling, we examined activation status of signaling molecules upon EPO stimulation, such as STAT5, ERK/MAPK, PI3K/AKT, and Bcl-X_L (Richmond et al., 2005; Socolovsky et al., 1999). Mice were treated with PHZ and $CD71^+$ splenic erythroblasts were harvested using magnetic beads. Cells were serum starved for 2 hr and then stimulated with EPO. We next assessed the phosphorylation status of Stat5 by Western blot and FACS. As shown in Figures S4A and S4B, activation of Stat5, ERK/MAPK and PI3K/AKT was induced normally upon EPO stimulation in pIpC-treated *Zbtb7a*$^{flox/-Mx1Cre+}$ erythroblasts, indicating that upstream EPO signaling is intact in the absence of *Lrf*. Furthermore, Bcl-X_L was abundantly expressed in pIpC-treated *Zbtb7a*$^{flox/-Mx1Cre+}$ erythroblasts (Figure S4C). Of note, the antiapoptotic protein Mcl1 was comparably expressed as well, whereas Bcl-2 protein was slightly reduced in *Zbtb7a*$^{flox/-Mx1Cre+}$ erythroblasts. Thus, erythroid apoptosis observed in *Lrf* conditional knockout mice is not due to an impaired EPO/EPO-R signaling pathway.

Upregulation of the Proapoptotic Factor Bim in the Absence of *Lrf*

In order to understand how loss of *Lrf* results in erythroblast apoptosis, we studied mRNA expression profiles in the R1 population of flow-sorted $CD71^+Ter119^-$ FL erythroblasts (Figure S5A). This population was selected for analysis because it consists of cells at a differentiation stage that did not exhibit overt cellular degeneration. A total of 189 probe sets were up or downregulated more than 1.5-fold in *Zbtb7a*$^{-/-}$ R1 cells as compared with *Zbtb7a*$^{+/+}$ and *Zbtb7a*$^{+/-}$ cells. From the list of genes thus compiled (see Figure S6), we selected genes that have been implicated in cellular apoptosis, differentiation, proliferation, and the cell cycle (Figure S5A). Many genes known to be involved in definitive erythropoiesis (Godin and Cumano, 2002) were expressed normally in *Zbtb7a*$^{-/-}$ R1 cells (Figure S5B). Interestingly, the BH3 only protein Bim (O'Connor et al., 1998) (encoded by *Bcl2l11* gene), a major apoptosis inducer in hematopoietic cells (Strasser et al., 1995), was found to be markedly upregulated with two independent probe sets in *Zbtb7a*$^{-/-}$ R1 cells (Figure S5A). Because apoptosis of *Zbtb7a*$^{-/-}$ FL erythroblasts was not reverted by *Arf/p53* loss and Bim is known to function in an Arf/p53-independent apoptosis pathway (Egle et al., 2004; Hemann et al., 2005), we investigated further the role of Bim in the defective erythropoiesis observed in the absence of *Lrf*. We found high *Bim* mRNA expression and an approximately 3-fold upregulation of Bim protein in flow-sorted $c\text{-}Kit^+CD71^+Ter119^-$ *Zbtb7a*$^{-/-}$ erythroblasts (Figure 3B and Figure 3C). Furthermore, Bim-EL protein levels were significantly elevated in $CD71^+$ pIpC-treated *Zbtb7a*$^{flox/-Mx1Cre+}$ splenic erythroblasts irrespective of EPO signals, whereas Bcl-X_L protein level was similar to that of control cells (Figure 3D). Markedly elevated Bim expression was also observed by immunohistochemistry in both *Zbtb7a*$^{-/-}$ 14.5 FL and pIpC-treated *Zbtb7a*$^{Flox/FloxMx1cre+}$ spleens (Figure 3E), indicating that Bim upregulation is a characteristic feature of *Lrf* loss both in the embryo and in the adult.

Bim Is a Direct Transcriptional Target of Lrf

Upregulation of *Bim* mRNA in *Lrf* deficient erythroblasts was due to an increase in transcription of the *Bim* gene rather than enhanced *Bim* mRNA stability, as reduction of Lrf expression via siRNA-mediated knockdown in erythroblasts did not affect *Bim* mRNA stability during erythroid differentiation (Figure S7A). In multiple cell types, Bim is regulated by the transcription factor Foxo3a downstream the PI3K/Akt pathway (Dijkers et al., 2000; Stahl et al., 2002). We therefore examined whether *Bim* upregulation in *Zbtb7a*$^{-/-}$ erythroblasts might be accompanied by an accumulation of Foxa3a protein in the nucleus. As shown in Figures S7B and S7C, no significant increase of nuclear Foxo3a protein was observed by immunohistochemistry (IHC) in either *Zbtb7a*$^{-/-}$ 15.5 FL or pIpC-treated *Zbtb7a*$^{flox/-Mx1Cre+}$ spleens, indicating that *Bim* upregulation in *Zbtb7a*$^{-/-}$ erythroblasts does not depend on Foxo3a.

Because LRF can act as a transcriptional repressor (Maeda et al., 2005), we next tested whether Lrf directly represses *Bim* transcription. To this end, we generated a set of luciferase reporter constructs containing regions of the proximal *Bim* promoter, and we assessed the ability of Lrf to repress reporter activity. As shown in Figure 3F, Lrf efficiently repressed activity of an 800 bp region of the *Bim* proximal promoter. Furthermore, by generating a series of deletions and truncations of this 800 bp fragment, we were able to identify a 250 bp region upstream of the *Bim* transcription start site that had promoter activity and was still sensitive to Lrf-mediated repression (Figure 3F). Within this 250 bp proximal promoter region we identified four potential LRF binding sites (Maeda et al., 2005) (Figure 3G). Although mutation of any single LRF binding site alone did not impair Lrf-mediated repression (data not shown), mutation of two adjacent sites close to the transcription start site abrogated Lrf-mediated repression (Figure 3G). Further, *Lrf* was found to directly bind to oligonucleotides that contain these putative LRF binding sites in the *Bim* gene as demonstrated by electrophoretic mobility shift assays. In addition, Lrf antibodies were found to super-shift the Lrf-oligonucleotide complex (Figures S8D and S8E). These data support a model whereby Lrf directly represses *Bim* expression through a tandem-binding site in the *Bim* proximal promoter region.

Chromatin immunoprecipitation (ChIP) experiments further demonstrated a direct binding of LRF on the Bim promoter. We designed two primer sets; one to amplify the proximal human *BIM* promoter and another to amplify the 5′ promoter of *HPRT1* as a negative control. LRF antibody specifically precipitated the proximal *BIM* promoter sequences from chromatin preparations of K562 erythroleukemia cells (Figure 3H). An important confirmation of this result was obtained by inducing differentiation of K562 cells with hemin (Figure 3H). (Rutherford et al., 1979). Under these conditions LRF is upregulated, and an enhanced enrichment of LRF at the *BIM* promoter was detected (Figure 3H). We conclude that LRF directly binds to the *BIM* promoter and inhibits its expression during erythroid differentiation.

Bim Deficiency Rescues the Anemia Observed in *Lrf*-Knockout Mice

In order to define more clearly the functional role of the Lrf-Bim interaction in suppressing apoptosis in erythroblasts, mice heterozygous for both *Lrf* and *Bim* genes (*Zbtb7a*$^{+/-}$*Bim*$^{+/-}$) were intercrossed to obtain *Lrf/Bim* double knockout embryos (*Zbtb7a*$^{-/-}$*Bim*$^{-/-}$). As shown in Figure 4A, while *Zbtb7a*$^{-/-}$ *Bim*$^{+/+}$ 15.5 d.p.c. embryos were overtly pale, *Zbtb7a*$^{-/-}$*Bim*$^{-/-}$

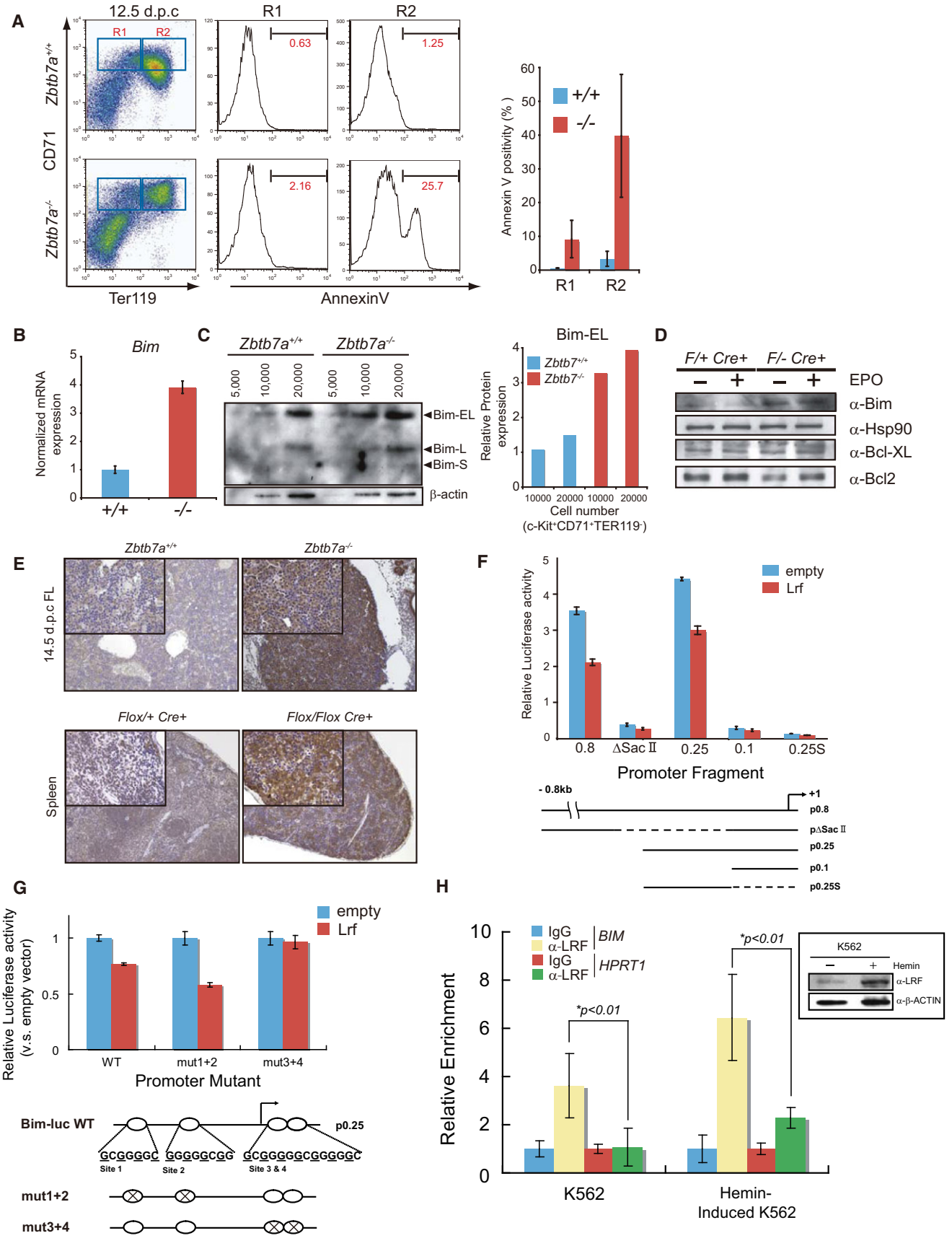
A
12.5 d.p.c
R1
R2
Zbtb7a+/+
Zbtb7a-/-
CD71
Ter119
AnnexinV
0.63
1.25
2.16
25.7
Annexin V positivity (%)
+/+
-/-
B
Bim
Normalized mRNA expression
C
Zbtb7a+/+
Zbtb7a-/-
5,000
10,000
20,000
Bim-EL
Bim-L
Bim-S
β-actin
Bim-EL
Relative Protein expression
Cell number
(c-Kit+CD71+TER119-)
D
F/+ Cre+
F/- Cre+
EPO
α-Bim
α-Hsp90
α-Bcl-XL
α-Bcl2
E
14.5 d.p.c FL
Spleen
Flox/+ Cre+
Flox/Flox Cre+
F
empty
Lrf
Relative Luciferase activity
0.8
ΔSac Ⅱ
0.25
0.1
0.25S
Promoter Fragment
- 0.8kb
+1
p0.8
pΔSac Ⅱ
p0.25
p0.1
p0.25S
G
empty
Lrf
Relative Luciferase activity (v.s. empty vector)
WT
mut1+2
mut3+4
Promoter Mutant
Bim-luc WT
p0.25
GCGGGGC
GGGGGCGG
GCGGGGGCGGGGGC
Site 1
Site 2
Site 3 & 4
mut1+2
mut3+4
H
IgG
α-LRF
BIM
HPRT1
*p<0.01
K562
Hemin
α-LRF
α-β-ACTIN
Relative Enrichment
K562
Hemin-
Induced K562

embryos appeared grossly normal. *Bim* deficiency significantly increased total numbers of FL (Figure 4B) and mature erythroblast (R3) cells in 12.5 d.p.c. and 14.5 d.p.c. embryos (Figures 4C, 4D, and S8A). In the double-knockout mice, Annexin V-positive apoptotic cells were nearly absent (Figures 4E, 4F, S8B, and S8C), providing proof that removal of *Bim* is sufficient to abrogate erythroblast apoptosis. Of note, *Zbtb7a*$^{-/-}$ embryos heterozygous for *Bim* (*Zbtb7a*$^{-/-}$*Bim*$^{+/-}$) displayed an intermediate phenotype (Figures 4B–4F). Thus, the rescue from fetal anemia of *Lrf* knockout mice through loss of *Bim* is gene-dosage dependent.

These data prompted us to analyze the effect of *Bim* loss on lethality seen in *Zbtb7a*$^{-/-}$ embryos. To this end, *Zbtb7a*$^{+/-}$ *Bim*$^{+/-}$ mice were intercrossed, and their progenies were analyzed at different embryonic days. *Zbtb7a*$^{-/-}$ embryos were alive at 14.5 d.p.c. irrespective of *Bim* genotype, but none of the *Zbtb7a*$^{-/-}$*Bim*$^{+/+}$ or *Zbtb7a*$^{-/-}$*Bim*$^{+/-}$ progenies were delivered (Table S1). However, 3 *Zbtb7a*$^{-/-}$*Bim*$^{-/-}$ pups out of 35 offspring analyzed were identified on the day of birth (P_0), indicating that complete loss of the *Bim* gene prolonged the survival of *Zbtb7a*$^{-/-}$ embryos (Table S1). These three *Zbtb7a*$^{-/-}$*Bim*$^{-/-}$ mice were nevertheless paler than controls at birth and subsequently died postnatally.

Overall, *Bim* loss was sufficient to restore nearly normal erythropoiesis in *Zbtb7a*$^{-/-}$ FL up to 14.5 d.p.c. and partially rescued lethality in *Zbtb7a*$^{-/-}$ embryos. Our genetic analysis thus indicates that excessive Bim expression is a primary cause of defective erythropoiesis in *Zbtb7a*$^{-/-}$ FLs.

Lrf Is a Direct Transcriptional Target of Gata1

The Gata1 transcription factor plays a central role in erythroid gene expression (Cantor and Orkin, 2002; Fujiwara et al., 1996) and protects erythroblasts from apoptosis (Weiss and Orkin, 1995; Gregory et al., 1999). We next examined Gata1 expression in pIpC-treated *Zbtb7a*$^{flox/-Mx1Cre+}$ CD71$^+$ erythroblasts. As shown in Figure 5A, Gata1 protein is abundantly expressed in pIpC-treated *Zbtb7a*$^{flox/-Mx1Cre+}$ CD71$^+$ erythroblasts.

LRF was recently identified as an EKLF-induced gene both in fetal liver cells and erythroid cell lines (Hodge et al., 2006). Because GATA1 is a transcriptional activator of *EKLF* (Crossley et al., 1994), and EKLF is indispensable for fetal erythropoiesis (Hodge et al., 2006; Perkins et al., 1995), we speculated that LRF is a key downstream target of the GATA1/EKLF transcriptional cascade enabling survival of differentiating erythroblasts. Indeed, while examining the promoter regions of the mouse *Zbtb7a* gene, we found two putative GATA binding sites and three EKLF consensus sequences (Figure 5B). Of note, the two putative GATA binding sites are fully conserved in the promoter region of the human *ZBTB7A* gene (not shown). To test whether Gata1 can activate *Lrf* expression, we used the *Gata1* null erythroid cell line G1E (Gregory et al., 1999). These cells proliferate as immature erythroblasts and undergo terminal maturation when Gata1 activity is restored. Upon activation of a drug-inducible form of Gata1, *Lrf* mRNA was upregulated approximately 4-fold (Figure 5C). We also observed upregulation of Eklf and Bcl-X_L and downregulation of Myb, as previously reported (Figure 5C) (Gregory et al., 1999; Welch et al., 2004).

We next examined whether Gata1 upregulates *Lrf* transcription via two putative GATA binding sites within the *Lrf* promoter. Dual-luciferase reporter assay experiments demonstrated that two Gata elements in the *Zbtb7a* gene act cooperatively to enhance promoter activity in murine erythroleukemia (MEL) cells (Figure 5D). To further elucidate the mechanism by which Gata1 induces Lrf, we performed ChIP experiments. Although we could not detect Eklf binding to the *Zbtb7a* promoter (Figures S9A and S9B), anti-Gata1 antibody specifically precipitated the ~400 bp proximal *Zbtb7a* promoter sequences, which contain the putative Gata1 binding sites, from extracts prepared from the induced G1E2-ER4 cells, but not from the parental cell line G1E2 (Rylski et al., 2003) (Figure 5E). As a further control, we could also efficiently enrich the *Fog1* promoter sequence using anti-Gata1 antibody (Welch et al., 2004) (Figure S9C). We obtained similar results in ChIP assays using MEL cells, an independent experimental system for in vitro erythroid differentiation (Figure 5F). These data indicate that Gata1 directly binds to the *Zbtb7a* proximal promoter in vivo and activates *Lrf* expression.

Figure 3. Loss of *Lrf* Leads to Increased Apoptosis Accompanied by High *Bim* Expression

(A) Representative FACS profiles of the triple staining for Ter119, CD71, and Annexin V (left). Bar graph demonstrates the average of percentage Annexin V positivity in R1 and R2 cell populations.

(B) *Bim* mRNA was increased in *Zbtb7a*$^{-/-}$ FL erythroblasts. c-Kit$^+$CD71$^+$Ter119$^-$ erythroblasts were flow sorted and RNA was extracted. cDNA was subsequently synthesized after DNase treatment and levels of *Bim* and *Hprt1* transcripts were measured by quantitative RT-PCR. Bar graph represents normalized expression level of *Bim* mRNA with error bars.

(C) Bim protein was upregulated in *Zbtb7a*$^{-/-}$ FL erythroblasts. Different numbers of c-Kit$^+$CD71$^+$Ter119$^-$ erythroblasts (5,000, 10,000, and 20,000) were directly flow-sorted into protein sample buffer and western blot was subsequently performed using anti-Bim antibody (left). Bar graph represents normalized Bim protein level to the corresponding β-actin protein levels in c-Kit$^+$CD71$^+$Ter119$^-$ erythroblasts from 12.5 d.p.c. FLs (right).

(D) High Bim protein expression in pIpC-treated *Zbtb7a*$^{Flox/-Mx1cre+}$ CD71$^+$ splenic erythroblasts. CD71$^+$splenic erythroblasts were harvested from PHZ-treated, pIpC-pretreated *Zbtb7a*$^{Flox/+Mx1cre}$ and *Zbtb7a*$^{Flox/-Mx1cre+}$ mice. Erythroblasts were then serum starved and subsequently stimulated with EPO. Cells were harvested 10 min after EPO administration and subsequently utilized for experiments.

(E) IHC analysis for Bim in FL and spleen. FLs were isolated from littermate embryos at 14.5 d.p.c. Spleens were collected 1 month after pIpC treatment. Both low-power magnification (×100) and high-power magnification (insets, ×400) are shown.

(F) Transrepression assays in 293 cells transfected with various luciferase reporter constructs of the murine proximal *Bim* promoter.

(G) Identification of an essential LRF-binding site in the murine *Bim* promoter. The putative LRF-binding sites in the *Bim* promoter were mutagenized and subsequently used for reporter assays. Schematic representations of mutated promoter and expression control for the reporter assay are shown (bottom). Underlined bases of the LRF-binding sites were mutated to adenine. Luciferase reporter plasmids were transfected into 293 cells. Luciferase activity was measured 24 hr after transfection using the Dual-Luciferase Reporter Assay system. Lrf did not repress the promoter activity of mut3+4 reporter.

(H) Quantitative ChIP assay of the *BIM* promoter both in K562 cells and in induced K562 cells by hemin. Primer sets were designated to amplify the proximal human *BIM* promoter and primers designated to the 5′ promoter of *HPRT1* were used to detect nonspecific interactions. The chromatin was sonicated to 200–600 bp. A western blot demonstrates that LRF is upregulated in induced K562 cells by hemin. All error bars indicate SD.

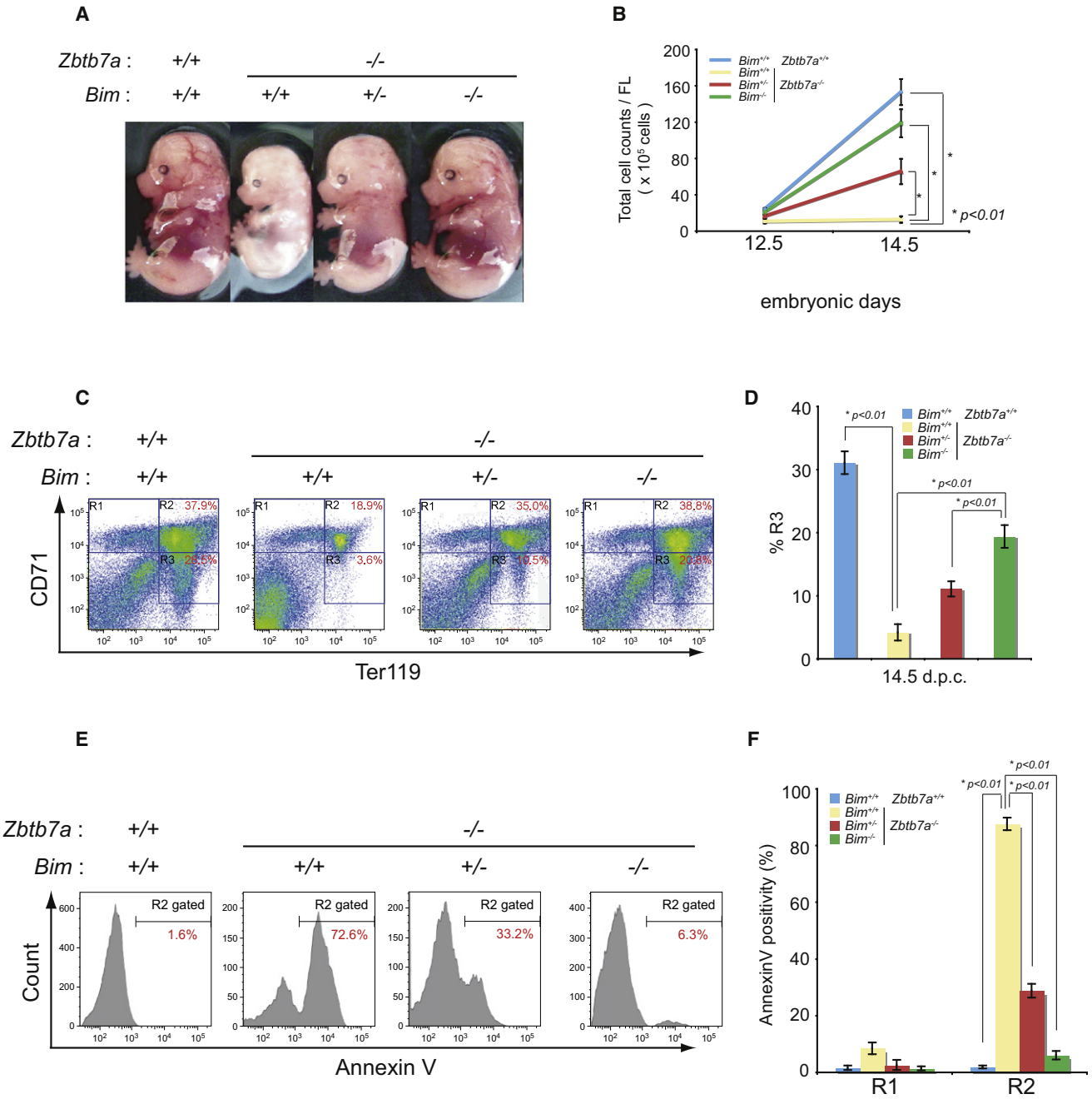

Figure 4. Loss of *Bim* Restores Erythropoiesis in *Zbtb7a*$^{-/-}$ FL

(A) Picture of *Zbtb7a Bim*$^{+/+}$, *Zbtb7a*$^{-/-}$*Bim*$^{+/-}$, and *Zbtb7a*$^{-/-}$*Bim*$^{-/-}$ 15.5 d.p.c. embryos.

(B) Total cell numbers per FL for each genotype at different embryonic days. Three litters were isolated for each time point and average numbers are presented with SD.

(C) Representative FACS profiles of 14.5 d.p.c. FLs from *Zbtb7a*$^{-/-}$*Bim*$^{+/+}$, *Zbtb7a*$^{-/-}$*Bim*$^{+/-}$, and *Zbtb7a*$^{-/-}$*Bim*$^{-/-}$ 14.5 d.p.c. embryos.

(D) Bar graph shows R3 population in 14.5 d.p.c. FLs. Three embryos were obtained and analyzed for each genotype.

(E) Representative FACS profiles of the staining for Annexin V in R2 cell population.

(F) Bar graph demonstrates the average of percentage Annexin V positivity in R1 and R2 cell populations. Three FLs were analyzed for each genotype. All error bars indicate SD.

We next asked whether Lrf overexpression restores terminal erythroid differentiation in the absence of *Gata1* using G1E-ER4 cells. We performed all experiments in the presence of EPO, because G1E-ER4 cells underwent apoptosis in the absence of EPO irrespective of Lrf levels (not shown). Retroviral overexpression of Lrf in G1E-ER4 cells led to an increase in Ter119-positive

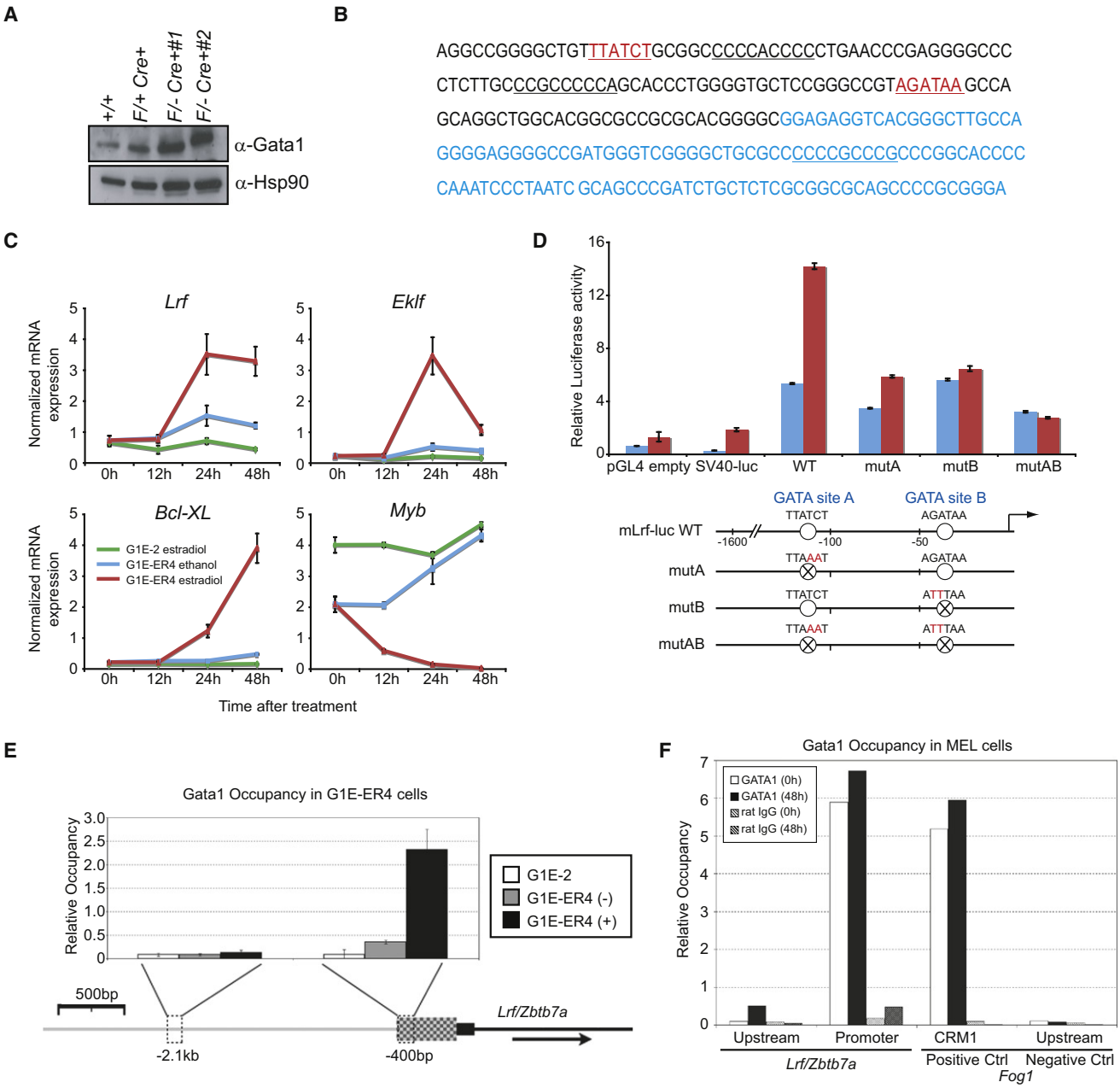

Figure 5. Lrf is a Gata1 Downstream Target

(A) Western blot for Gata1 in *Zbtb7a*$^{+/+}$, *Zbtb7a*$^{Flox/+Mx1cre}$, and *Zbtb7a*$^{Flox/-Mx1cre+}$ CD71^{+} splenic erythroblasts. Gata1 was abundantly expressed in the absence of *Lrf*.

(B) Sequence of 450 bases of the predicted promoter region of the *Zbtb7a* gene. Consensus EKLF CACCC boxes are underlined; consensus GATA1 binding motifs are depicted in red and underlined; exon 1 sequence is shown in blue.

(C) G1E-ER4 is a *Gata1*-ablated erythroblast line expressing an estradiol-inducible form of GATA1. G1E-ER4 cells and its parental cell line G1E-2 were stimulated with 10^{-7} M estradiol or ethanol vehicle and RNA was extracted at the indicated times after stimulation. mRNA levels of *Lrf*, *Eklf*, *Bcl-X*$_L$, and *Myb* were measured by quantitative RT-PCR and normalized to the corresponding *Hprt1* mRNA levels.

(D) Two GATA elements in the *Zbtb7a* gene act cooperatively to enhance promoter activity in erythroid cells.

(E) Quantitative ChIP assay at the *Lrf* promoter in *Gata1* null parental (G1E-2), uninduced (–), and induced (+) G1E-ER4 cells using anti-Gata1 antibody. The *y* axis shows Gata1 occupancy, relative to a standard curve of the relevant input sample. Below, diagram of the 5′ end of the *Zbtb7a* gene. Thin black line indicates intron 1; black box represents exon 1; checkered box represents the predicted promoter region, which contains 2 consensus GATA1 binding sites and 3 consensus EKLF CACCC boxes; thin gray line represents the upstream intergenic region. Dashed boxes show regions amplified by quantitative RT-PCR for ChIP. Arrow indicates direction of transcription.

(F) Quantitative ChIP assay using anti-GATA1 antibody in MEL cells chemically induced to differentiate for either 0 hr or 48 hr. Data from immunoprecipitations performed with normal rat immunoglobin G are shown as controls. All error bars indicate SD.

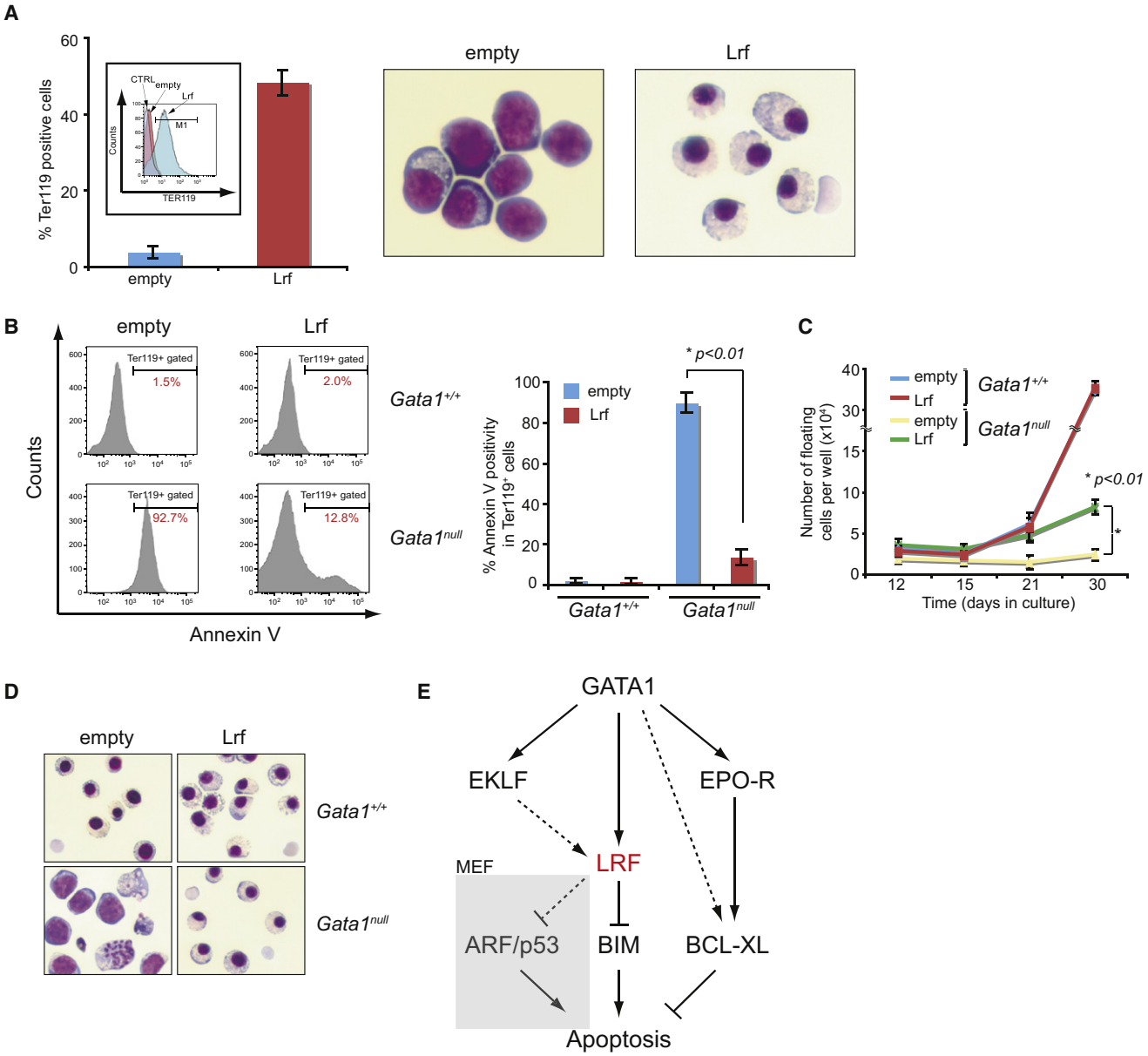

Figure 6. Lrf Overexpression Restores Erythroid Differentiation in *Gata1*-Deficient Erythroblasts

(A) Proportions of Ter119-positive G1E-ER4 cells upon *Lrf* overexpression without estradiol treatment (left). Representative FACS profiles for Ter119 expression is also demonstrated with isotype control (left). Pictures demonstrate cytospin preparations of G1E-ER4 cells expressing empty vector or Lrf (right).

(B) *Gata1* wild-type and null ES cells expressing either empty vector or *Lrf* were induced toward erythroid differentiation on OP9 stromal layers. Floating hematopoietic cells were harvested and analyzed. Representative FACS profiles of the staining for Annexin V in Ter119-positive cell population (left). Bar graph demonstrates the average of percentage Annexin V positivity in Ter119-positive cell fraction (right).

(C) Sequential analysis for the numbers of floating blood cells derived from *Gata1* null ES cells expressing either empty vector (yellow) or *Lrf* (green).

(D) May-Giemsa staining of floating erythrocytes (×400 magnification).

(E) Proposed model of the role for LRF in terminal erythroid differentiation. We propose that inhibition of apoptosis during erythroid terminal differentiation is dependent on both the EPO/BCL-XL and the LRF/BIM pathways, which are activated in response to the transcription factor GATA1. Loss of the tumor suppressor *Arf* reverted the senescence phenotype in *Zbtb7a*$^{-/-}$ MEFs (Maeda et al., 2005). All error bars indicate SD.

erythrocytes (Figure 6A), accompanied by a reduction in *Bim* mRNA levels (Figure S10A). Lrf-overexpressing G1E-ER4 cells formed hemoglobinized erythroid colonies without Gata1 induction when seeded in methylcellulose plates (Figure S10B). Conversely, siRNA-mediated *Lrf* knockdown resulted in increase of apoptosis revealed by morphological examination (Figure S10C) and Annexin V staining (Figure S10D). Successful *Lrf* knockdown in siRNA-treated cells was confirmed by western blot (Figure S10E). Furthermore, as expected, we observed a significant increase of apoptotic erythroblasts when *Bim* was

ectopically expressed in differentiating G1E-ER4 cells (Figures S10F and S10G). Of note, the proapoptotic effects of *Lrf* knock down as well as Bim overexpression became evident once differentiation was initiated by Gata1 induction. This suggests that Bim repression by Lrf is chiefly required in late stages of erythroid differentiation, which is in complete agreement with our findings in *Lrf* knockout mice.

To confirm our findings in primary cells, we next took advantage of an OP9/mouse embryonic stem cell (ESC) coculture system. We overexpressed Lrf in *Gata1* null ES cells and examined erythroid differentiation (Weiss et al., 1994). In this system, ES cells give rise to a nonadherent hematopoietic cell population that includes erythrocytes (Umeda et al., 2004; Umeda et al., 2006). Nonadherent cells were harvested serially and Annexin V positivity within the Ter119-positive fraction was analyzed. Lrf overexpression significantly augmented their survival (Figure 6B) and increased the production of nonadherent cells, which consisted mainly of Ter119 erythroblasts (Figures 6C, 6D, and S10H). Thus, overexpression of Lrf partially overrides erythroblast apoptosis and maturation arrest caused by lack of *Gata1*.

DISCUSSION

The transcription factor LRF has previously been identified as a regulator of the important tumor suppressor ARF, and cells lacking *Lrf* have proved refractory to malignant transformation (Maeda et al., 2005). LRF also plays an essential role in the B versus T lymphoid cell-fate decision (Maeda et al., 2007): thus, the gene encoding Lrf, *Zbtb7a*, belongs to the select group of genes that have a crucial role in both oncogenesis and development. In this work we have shown that the latter role includes a function that is essential for erythropoiesis, and we defined the mechanism whereby this function is fulfilled.

First, we have established that LRF plays a key role in fetal and adult erythropoiesis. $Zbtb7a^{-/-}$ embryos die of severe anemia by 16.5 d.p.c.; and in adult mice conditional inactivation of *Lrf* in HSCs results in an EPO-unresponsive macrocytic anemia due to a cell intrinsic defect. Through targeted inactivation, a number of other genes have been previously identified as key factors in definitive erythropoiesis (Godin and Cumano, 2002). Upon EPO-R activation, STAT5 is phosphorylated, translocates to the nucleus, and induces transcriptional activation of target genes. Inactivation of both isoforms of *Stat5* in mice ($Stat5a^{-/-}Stat5b^{-/-}$) results in inefficient erythropoiesis in both the fetus and the adult organism (Socolovsky et al., 2001). We find similar phenotypic features in *Lrf* conditional knockout mice, despite the fact that *Lrf* null erythroblasts have an intact EPO-STAT5 signaling pathway. Indeed, Bcl-X_L, a downstream target of Stat5, is normally induced upon EPO stimulation in the absence of *Lrf* (Figure S4C); and the MAPK and PI3K pathways, which are also downstream of the EPO receptor, are activated normally in *Lrf* null erythroblasts (Figure S4B). Thus, the role of LRF in terminal erythroid differentiation does not appear to be related to the EPO signaling cascade.

We have shown previously that LRF blocks the Notch pathway in HSC/progenitor cells to regulate B versus T lineage fate decision (Maeda et al., 2007). However, the defect in erythroid differentiation in *Lrf* knockout mice was not rescued by inhibition of Notch activity by treatment in vivo with a gamma secretase inhibitor (Figure S11). Furthermore, a Notch activation signature is not present in *Lrf* knockout MEP in contrast to our findings in HSC/CLPs (common lymphoid progenitors) (Maeda et al., 2007). Thus, failure of erythropoiesis upon loss of *Lrf* cannot be accounted for by aberrant Notch activation.

Our next key finding was that *Lrf* loss causes apoptosis of erythroblasts, mostly at the transition from the basophilic to the polychromatophilic stage. The ARF/p53 pathway is critical in the induction of apoptosis, cell cycle arrest, and cellular senescence in response to oncogenic stress (Lowe and Sherr, 2003). High p53 expression induces apoptosis in fetal liver erythroblasts and erythroid-specific inactivation of the mouse *Mdm2* gene, a key negative regulator of p53, leads to increased apoptosis in erythroblasts and embryonic lethality due to a severe anemia ($Mdm2^{lox/lox}EpoR^{cre+}$) (Maetens et al., 2007). However, neither *Arf* loss nor *p53* loss could rescue the defects in *Lrf* null erythroblasts (Figure S3 A–C): in other words, apoptosis of *Lrf* null erythroblasts was Arf/p53 independent.

The mechanism whereby *Lrf* loss produces apoptosis was clarified by analyzing the gene expression profile of *Lrf* null cells by microarray. We focused on the fact that in *Lrf* null cells the proapoptotic factor Bim was markedly upregulated at the level of both mRNA and protein (Figures 3B–3E). Reporter assays and ChIP experiments demonstrated that LRF physically binds to the *BIM* promoter and directly represses transcription of this gene (Figures 3F–3H). Probably the most convincing evidence that Lrf function is linked to Bim comes from our genetic analysis: if *Bim* is knocked out, the severe erythroid cell phenotype of $Zbtb7a^{-/-}$ mutants, including lethal anemia, is almost completely reversed (Figures 4 and S8). The rescue is gene-dosage dependent, because loss of even one *Bim* allele provides a significant survival advantage to $Zbtb7a^{-/-}$ erythroblasts (Figures 4 and S8). Our data indicate that "fine-tuning" of Bim levels via Lrf is key for erythroblast survival. BIM was already known to function in an ARF/p53-independent apoptosis pathway (Egle et al., 2004; Hemann et al., 2005). An important implication of our work is that both p53- and Bim-dependent apoptotic pathways must be suppressed for effective erythroid differentiation.

Finally, we have discovered that LRF is a novel direct transcriptional target of *GATA1*. *Lrf* mRNA expression was induced upon *Gata1* re-expression in a *Gata1* null erythroblast cell line (Figure 5C), and by ChIP analysis Gata1 is found to directly bind to the *Lrf* promoter in vivo (Figures 5E and 5F). Gata1 expression is barely detectable at HSC/progenitor stages and is upregulated during erythroid lineage commitment, being expressed at the highest levels in CFU-E and in proerythroblasts (Suzuki et al., 2003). *Gata1* null embryonic stem cells fail to produce mature erythroid cells in vivo in chimeric mice (Pevny et al., 1991) due to massive apoptosis of erythroblasts (Weiss et al., 1994), demonstrating Gata1's essential role as a survival factor during this differentiation process. In this context, our study identifies LRF as a key downstream target of GATA1. In agreement with this notion, forced Lrf overexpression in *Gata1* null cells led to *Bim* downregulation and prolonged the survival of *Gata1* null erythroblasts (Figures 6 and S10H), enabling erythroid cells to undergo terminal maturation at least to some extent.

The differentiation and maturation of erythroid cells is a highly regulated process: in its terminal stages, it exhibits features of apoptosis (Weiss and Orkin, 1995; Gregory et al., 1999; Socolovsky et al., 1999; Yoshida et al., 2005). If apoptosis is abnormally triggered at earlier stages of differentiation, the output of mature erythrocytes will be compromised: this underlies the phenomenon of intramedullary destruction of red cell precursors known as ineffective erythropoiesis, which causes anemia in inherited disorders such as thalassemia (Rivella, 2009; Wu et al., 2005). Here we have shown that control of the proapoptotic protein BIM is critical for normal erythropoiesis: and this control is exerted by LRF. If we consider hematopoiesis as a whole, we can speculate that although BIM is essential in lymphoid cells for preventing autoimmunity (Bouillet et al., 1999), it is essential that BIM activity be curbed in erythroid cells. This notion fits well with the important finding that production of LRF itself is activated by GATA1, a master gene of erythropoiesis (Figure 6E). Finally, our findings also have important implications for the role of LRF in tumorigenesis because they identify yet another critical mechanism (the ability to repress BIM with the consequent survival advantage) whereby LRF can lend to the oncogenic potential of tumor cells.

EXPERIMENTAL PROCEDURES

Mice

Generation of conventional (*Zbtb7a*$^{+/-}$) and conditional (*Zbtb7a*$^{Flox/+}$) *Lrf* knockout mice was described elsewhere (Maeda et al., 2007). *Mx1-Cre* transgenic mice (Gu et al., 1994), *Bim* (*Bcl2l11*) knockout mice (Bouillet et al., 1999), and the congenic strain that carries the CD45.1 antigen (B6.SJL-*Ptprc*^{a}*Pepc*^{b}/BoyJ) were purchased from Jackson Laboratory.

Analysis of Embryonic PB and Colony Forming Assay

PB was collected with a micropipette from the carotid arteries of embryos and smears were prepared for Wright-Giemsa staining. Hematocrit was determined using microhematocrit tubes (Microcaps, Drummond Scientific). FL colony-forming assays in methylcellulose were performed as previously described (Wang et al., 1998). For the CFU-E colony assay in *Lrf* conditional knockout mice, 10,000 flow-sorted the MEPs were cultured in EPO-containing methylcellulose plates (MethoCult M3334, StemCell Technologies) for 2 days and colony numbers were subsequently counted.

FACS and Cell Purification

After blocking nonspecific antibody binding by incubating with FcBlock (BD), FL and BM cells were incubated with fluorochrome-conjugated (or with biotin-conjugated) antibodies. FACS analysis was performed in FACScan, FACSCalibur, or CyAn (DAKO), followed by analysis with FlowJo software (Tree Star). Cell sorting was performed on a MoFlo at MSKCC and BIDMC Flow Cytometry Core Facility using DAPI for live/dead discrimination. Antibodies for FACS and cell sorting were purchased from eBioscience unless otherwise indicated. FACS analysis for Phospho-Stat5 was performed according to the phospho-FACS protocol from the lab of Dr. Kevin Shannon (http://www.ucsf.edu/kmslab/resources/resources.html) using AlexaFluor647-conjugated anti-PhosphoStat5 antibody (pY694, clone47, BD). For cell cycle analysis, DRAQ5 (Axxora) was added to a final concentration of 10 μM and cells were subsequently incubated for 10 min at room temperature. For Annexin V staining, FL cells were suspended with 1 x Annexin Biding Buffer (BD) containing 2% fetal bovine serum, stained with FITC-anti-CD71, PE-anti-Ter119 antibodies, and APC-Annexin V (BD) following the manufacturer's protocol.

Conditional Inactivation of *Lrf* and PB Analysis in Adult Mice

Cre recombinase was induced at the HSC level as previously described (Gu et al., 1994). PB samples were collected from the retro-orbital sinus with heparinized capillary tubes (Fisher Scientific) under isoflurane anesthesia. RBC counts, hematocrit, hemoglobin, and MCV were measured using an Adivia 120 hematology analyzer (Bayer). Serum erythropoietin level was measured using the Mouse/Rat Erythropoietin Quantikine ELISA Kit (R&D Systems).

PHZ Treatment and Collection of Splenic Erythroblasts

Phenylhydrazine (PHZ) was purchased from Sigma and injected subcutaneously three times at the dose of 40 mg/kg as previously described (Socolovsky et al., 2001). For CD71^{+} splenic erythroblast collection, the spleen was isolated at day 4 after PHZ stimulation and cells were then incubated with anti-CD71 biotin conjugated antibody (C2, BD), followed by incubation with anti-Biotin MicroBeads (Miltenyi Biotec). The cell suspension was subsequently applied onto MACS separation LS columns (Miltenyi Biotec) for positive selection.

Microarray Analysis

One *Zbtb7a*$^{+/+}$, one *Zbtb7a*$^{+/-}$, and two *Zbtb7a*$^{-/-}$ 12.5 d.p.c. FLs were isolated from littermate embryos. RNA of CD71^{+}Ter119^{-} erythroblasts was extracted according to the manufacturer's specifications. cDNA synthesis, cRNA labeling, and hybridization onto GeneChip Mouse Genome 430A2.0 chips (Affymetrix) was performed as previously described (Costoya et al., 2004). Because *Zbtb7a*$^{+/-}$ mice do not demonstrate any gross defect, we divided samples into two groups. Data sets from one *Zbtb7a*$^{+/+}$ and one *Zbtb7a*$^{+/-}$ samples were defined as a control group and the data sets from two *Zbtb7a*$^{-/-}$ samples were defined as a knockout group. Raw expression data on each chip was generated utilizing the Affymetrix Microarray Suite 5.0. Genes whose normalized data value were greater or less by more than 1.5-fold between two groups were selected and further evaluated statistically (Parametric test using Welch's approximate t test, with p value cutoff of 0.05) using GeneSpring software (SiliconGenetics).

In Vitro Hematopoietic Differentiation of Mouse Embryonic Stem Cells

Wild-type and *Gata1* null ES cells (Weiss et al., 1994; Pevny et al., 1991) were retrovirally infected with mock or *Lrf*-expressing vector followed by selection with puromycin on gelatinized dish. In vitro differentiation of ESCs, cell sorting, and colony-forming assays were performed as reported previously (Umeda et al., 2004, 2006). Floating hematopoietic cells that emerged after cell sorting were processed every 3 days for May-Giemsa staining as described previously (Umeda et al., 2004, 2006).

Identification of Potential *cis*-Regulatory Elements

To identify regions to be analyzed by ChIP, we examined the *Lrf* genomic locus in the UCSC Genome Browser along with a custom track showing erythroid predicted *cis*-regulatory modules (preCRMs) (Wang et al., 2006). Erythroid preCRMs are regions of high regulatory potential (Elnitski et al., 2003) containing at least one conserved consensus GATA1 binding motif (WGATAR). A 435 bp preCRM was identified immediately upstream of the start of transcription. Examination of the preCRM in the murine *Lrf* promoter revealed 2 consensus GATA1 binding motifs (WGATAR) and 3 consensus EKLF binding motifs (CCNCNCCCN).

Lrf Promoter Reporter Assay

Two milligrams of Lrf-PGL-4 reporter plasmid and 0.2 mg Renilla luciferase reporter plasmid (pRL) were transfected into MEL cells using Lipofectamine LTX+ Plus reagents (Invitrogen). Where indicated, MEL cells were induced toward erythroid maturation by addition of 5 mM hexamethylene bisacetamide for 72 hr prior to transfection. Luciferase activity was measured 24 hr after transfection using the Dual-Luciferase Reporter Assay system (Promega). Reported luciferase activities are normalized for transfection efficiency according to Renilla activities.

Bim Promoter Reporter Assay

pGL3-mBim0.8 reporter plasmid, containing 800 bp region immediately upstream of exon 1 of mouse Bim gene, was generated from the p0.8 vector (kind gift from Dr. Jerry M. Adams) (Bouillet et al., 2001). Truncated mutants (pΔSacII, p0.25, p0.1 and p0.25S) were generated by enzyme digestion. Mutagenesis was then performed using a Change-IT mutagenesis kit (USB Corporation, Cleveland, OH).

SUPPLEMENTAL DATA

Supplemental Data include 11 figures and a table and can be found with this article online at http://www.cell.com/developmental-cell/supplemental/S1534-5807(09)00387-6.

ACKNOWLEDGMENTS

We thank Agnes Viale and Julia Zhao for their help with microarray experiments; Irena Linkov and Katia Manova for IHC analysis; Bernessa Vassall for May-Giemsa staining; Jia-Hui Dong for performing mice work; Jan Hendrikx and other MSKCC Flow Cytometry core facility members for assistance with FACS analysis and cell sorting; Yu Yao for performing *Lrf* promoter Reporter assay; Ainara Egia for histology and IHC assistance; Nicola Hawe, Carmela Gurrieri, Jose Costoya, Francesco Piazza, Luipa Khandker, Ilhem Guernah, Kyoko Ito, Linda DiSantis, Stuart Megan, Thomas Naughton, and other P.P.P. lab members for assistance, advice, and helpful discussion. We also thank Margaret VanMeter for providing us with the Phospho Stat5 FACS protocol. This work is supported in part by NCI grant CA-102142 (to P.P.P.).

Received: April 26, 2009
Revised: June 11, 2009
Accepted: September 18, 2009
Published: October 19, 2009

REFERENCES

Bouillet, P., Zhang, L.C., Huang, D.C., Webb, G.C., Bottema, C.D., Shore, P., Eyre, H.J., Sutherland, G.R., and Adams, J.M. (2001). Gene structure alternative splicing, and chromosomal localization of pro-apoptotic Bcl-2 relative Bim. Mamm. Genome *12*, 163–168.

Bouillet, P., Metcalf, D., Huang, D.C., Tarlinton, D.M., Kay, T.W., Kontgen, F., Adams, J.M., and Strasser, A. (1999). Proapoptotic Bcl-2 relative Bim required for certain apoptotic responses, leukocyte homeostasis, and to preclude autoimmunity. Science *286*, 1735–1738.

Cantor, A.B., and Orkin, S.H. (2002). Transcriptional regulation of erythropoiesis: an affair involving multiple partners. Oncogene *21*, 3368–3376.

Costoya, J.A., Hobbs, R.M., Barna, M., Cattoretti, G., Manova, K., Sukhwani, M., Orwig, K.E., Wolgemuth, D.J., and Pandolfi, P.P. (2004). Essential role of Plzf in maintenance of spermatogonial stem cells. Nat. Genet. *36*, 653–659.

Crossley, M., Tsang, A.P., Bieker, J.J., and Orkin, S.H. (1994). Regulation of the erythroid Kruppel-like factor (EKLF) gene promoter by the erythroid transcription factor GATA-1. J. Biol. Chem. *269*, 15440–15444.

Davies, J.M., Hawe, N., Kabarowski, J., Huang, Q.H., Zhu, J., Brand, N.J., Leprince, D., Dhordain, P., Cook, M., Morriss-Kay, G., and Zelent, A. (1999). Novel BTB/POZ domain zinc-finger protein, LRF, is a potential target of the LAZ-3/BCL-6 oncogene. Oncogene *18*, 365–375.

Dijkers, P.F., Medema, R.H., Lammers, J.W., Koenderman, L., and Coffer, P.J. (2000). Expression of the pro-apoptotic Bcl-2 family member Bim is regulated by the forkhead transcription factor FKHR-L1. Curr. Biol. *10*, 1201–1204.

Egle, A., Harris, A.W., Bouillet, P., and Cory, S. (2004). Bim is a suppressor of Myc-induced mouse B cell leukemia. Proc. Natl. Acad. Sci. USA *101*, 6164–6169.

Elnitski, L., Hardison, R.C., Li, J., Yang, S., Kolbe, D., Eswara, P., O'Connor, M.J., Schwartz, S., Miller, W., and Chiaromonte, F. (2003). Distinguishing regulatory DNA from neutral sites. Genome Res. *13*, 64–72.

Fridman, J.S., and Lowe, S.W. (2003). Control of apoptosis by p53. Oncogene *22*, 9030–9040.

Fujiwara, Y., Browne, C.P., Cunniff, K., Goff, S.C., and Orkin, S.H. (1996). Arrested development of embryonic red cell precursors in mouse embryos lacking transcription factor GATA-1. Proc. Natl. Acad. Sci. USA *93*, 12355–12358.

Godin, I., and Cumano, A. (2002). The hare and the tortoise: an embryonic haematopoietic race. Nat. Rev. Immunol. *2*, 593–604.

Gregory, T., Yu, C., Ma, A., Orkin, S.H., Blobel, G.A., and Weiss, M.J. (1999). GATA-1 and erythropoietin cooperate to promote erythroid cell survival by regulating bcl-xL expression. Blood *94*, 87–96.

Gu, H., Marth, J.D., Orban, P.C., Mossmann, H., and Rajewsky, K. (1994). Deletion of a DNA polymerase beta gene segment in T cells using cell type-specific gene targeting. Science *265*, 103–106.

He, X., Dave, V.P., Zhang, Y., Hua, X., Nicolas, E., Xu, W., Roe, B.A., and Kappes, D.J. (2005). The zinc finger transcription factor Th-POK regulates CD4 versus CD8 T-cell lineage commitment. Nature *433*, 826–833.

Hemann, M.T., Bric, A., Teruya-Feldstein, J., Herbst, A., Nilsson, J.A., Cordon-Cardo, C., Cleveland, J.L., Tansey, W.P., and Lowe, S.W. (2005). Evasion of the p53 tumour surveillance network by tumour-derived MYC mutants. Nature *436*, 807–811.

Hodge, D., Coghill, E., Keys, J., Maguire, T., Hartmann, B., McDowall, A., Weiss, M., Grimmond, S., and Perkins, A. (2006). A global role for EKLF in definitive and primitive erythropoiesis. Blood *107*, 3359–3370.

Kuhn, R., Schwenk, F., Aguet, M., and Rajewsky, K. (1995). Inducible gene targeting in mice. Science *269*, 1427–1429.

Kukita, A., Kukita, T., Ouchida, M., Maeda, H., Yatsuki, H., and Kohashi, O. (1999). Osteoclast-derived zinc finger (OCZF) protein with POZ domain, a possible transcriptional repressor, is involved in osteoclastogenesis. Blood *94*, 1987–1997.

Lowe, S.W., and Sherr, C.J. (2003). Tumor suppression by Ink4a-Arf: progress and puzzles. Curr. Opin. Genet. Dev. *13*, 77–83.

Maeda, T., Hobbs, R.M., Merghoub, T., Guernah, I., Zelent, A., Cordon-Cardo, C., Teruya-Feldstein, J., and Pandolfi, P.P. (2005). Role of the proto-oncogene Pokemon in cellular transformation and ARF repression. Nature *433*, 278–285.

Maeda, T., Merghoub, T., Hobbs, R.M., Dong, L., Maeda, M., Zakrzewski, J., van den Brink, M.R., Zelent, A., Shigematsu, H., Akashi, K., et al. (2007). Regulation of B versus T lymphoid lineage fate decision by the proto-oncogene LRF. Science *316*, 860–866.

Maetens, M., Doumont, G., Clercq, S.D., Francoz, S., Froment, P., Bellefroid, E., Klingmuller, U., Lozano, G., and Marine, J.C. (2007). Distinct roles of Mdm2 and Mdm4 in red cell production. Blood *109*, 2630–2633.

O'Connor, L., Strasser, A., O'Reilly, L.A., Hausmann, G., Adams, J.M., Cory, S., and Huang, D.C. (1998). Bim: a novel member of the Bcl-2 family that promotes apoptosis. EMBO J. *17*, 384–395.

Pevny, L., Simon, M.C., Robertson, E., Klein, W.H., Tsai, S.F., D'Agati, V., Orkin, S.H., and Costantini, F. (1991). Erythroid differentiation in chimaeric mice blocked by a targeted mutation in the gene for transcription factor GATA-1. Nature *349*, 257–260.

Perkins, A.C., Sharpe, A.H., and Orkin, S.H. (1995). Lethal beta-thalassaemia in mice lacking the erythroid CACCC-transcription factor EKLF. Nature *375*, 318–322.

Pessler, F., Pendergrast, P.S., and Hernandez, N. (1997). Purification and characterization of FBI-1, a cellular factor that binds to the human immunodeficiency virus type 1 inducer of short transcripts. Mol. Cell. Biol. *17*, 3786–3798.

Rivella, S. (2009). Ineffective erythropoiesis and thalassemias. Curr. Opin. Hematol. *16*, 187–194.

Richmond, T.D., Chohan, M., and Barber, D.L. (2005). Turning cells red: signal transduction mediated by erythropoietin. Trends Cell Biol. *15*, 146–155.

Rutherford, T.R., Clegg, J.B., and Weatherall, D.J. (1979). K562 human leukaemic cells synthesise embryonic haemoglobin in response to haemin. Nature *280*, 164–165.

Rylski, M., Welch, J.J., Chen, Y.Y., Letting, D.L., Diehl, J.A., Chodosh, L.A., Blobel, G.A., and Weiss, M.J. (2003). GATA-1-mediated proliferation arrest during erythroid maturation. Mol. Cell. Biol. *23*, 5031–5042.

Socolovsky, M., Fallon, A.E., Wang, S., Brugnara, C., and Lodish, H.F. (1999). Fetal anemia and apoptosis of red cell progenitors in Stat5a−/−5b−/− mice: a direct role for Stat5 in Bcl-X(L) induction. Cell *98*, 181–191.

Socolovsky, M., Nam, H., Fleming, M.D., Haase, V.H., Brugnara, C., and Lodish, H.F. (2001). Ineffective erythropoiesis in Stat5a(−/−)5b(−/−) mice due to decreased survival of early erythroblasts. Blood *98*, 3261–3273.

Stahl, M., Dijkers, P.F., Kops, G.J., Lens, S.M., Coffer, P.J., Burgering, B.M., and Medema, R.H. (2002). The forkhead transcription factor FoxO regulates transcription of p27Kip1 and Bim in response to IL-2. J. Immunol. *168*, 5024–5031.

Stogios, P.J., Downs, G.S., Jauhal, J.J., Nandra, S.K., and Prive, G.G. (2005). Sequence and structural analysis of BTB domain proteins. Genome Biol. *6*, R82.

Strasser, A., Harris, A.W., Huang, D.C., Krammer, P.H., and Cory, S. (1995). Bcl-2 and Fas/APO-1 regulate distinct pathways to lymphocyte apoptosis. EMBO J. *14*, 6136–6147.

Suzuki, N., Suwabe, N., Ohneda, O., Obara, N., Imagawa, S., Pan, X., Motohashi, H., and Yamamoto, M. (2003). Identification and characterization of 2 types of erythroid progenitors that express GATA-1 at distinct levels. Blood *102*, 3575–3583.

Umeda, K., Heike, T., Yoshimoto, M., Shiota, M., Suemori, H., Luo, H.Y., Chui, D.H., Torii, R., Shibuya, M., Nakatsuji, N., and Nakahata, T. (2004). Development of primitive and definitive hematopoiesis from nonhuman primate embryonic stem cells in vitro. Development *131*, 1869–1879.

Umeda, K., Heike, T., Yoshimoto, M., Shinoda, G., Shiota, M., Suemori, H., Luo, H.Y., Chui, D.H., Torii, R., Shibuya, M., et al. (2006). Identification and characterization of hemoangiogenic progenitors during cynomolgus monkey embryonic stem cell differentiation. Stem Cells *24*, 1348–1358.

Wang, H., Zhang, Y., Cheng, Y., Zhou, Y., King, D.C., Taylor, J., Chiaromonte, F., Kasturi, J., Petrykowska, H., Gibb, B., et al. (2006). Experimental validation of predicted mammalian erythroid cis-regulatory modules. Genome Res. *16*, 1480–1492.

Wang, Z.G., Delva, L., Gaboli, M., Rivi, R., Giorgio, M., Cordon-Cardo, C., Grosveld, F., and Pandolfi, P.P. (1998). Role of PML in cell growth and the retinoic acid pathway. Science *279*, 1547–1551.

Weiss, M.J., Keller, G., and Orkin, S.H. (1994). Novel insights into erythroid development revealed through in vitro differentiation of GATA-1 embryonic stem cells. Genes Dev. *8*, 1184–1197.

Weiss, M.J., and Orkin, S.H. (1995). Transcription factor GATA-1 permits survival and maturation of erythroid precursors by preventing apoptosis. Proc. Natl. Acad. Sci. USA *92*, 9623–9627.

Welch, J.J., Watts, J.A., Vakoc, C.R., Yao, Y., Wang, H., Hardison, R.C., Blobel, G.A., Chodosh, L.A., and Weiss, M.J. (2004). Global regulation of erythroid gene expression by transcription factor GATA-1. Blood *104*, 3136–3147.

Wu, C.J., Krishnamurti, L., Kutok, J.L., Biernacki, M., Rogers, S., Zhang, W., Antin, J.H., and Ritz, J. (2005). Evidence for ineffective erythropoiesis in severe sickle cell disease. Blood *106*, 3639–3645.

Wu, H., Liu, X., Jaenisch, R., and Lodish, H.F. (1995). Generation of committed erythroid BFU-E and CFU-E progenitors does not require erythropoietin or the erythropoietin receptor. Cell *83*, 59–67.

Yoshida, H., Kawane, K., Koike, M., Mori, Y., Uchiyama, Y., and Nagata, S. (2005). Phosphatidylserine-dependent engulfment by macrophages of nuclei from erythroid precursor cells. Nature *437*, 754–758.